remote sensing

MDPI

Article

Multi-Instrumental Observations of Midlatitude Plasma Irregularities over Eastern Asia during a Moderate Magnetic Storm on 16 July 2003

Hailun Ye [1,2], Wen Yi [1,2], Baozhu Zhou [1,2], Jianfei Wu [1,2,3], Bingkun Yu [4], Penghao Tian [1,2], Jianyuan Wang [1,2], Chi Long [5], Maolin Lu [1,2], Xianghui Xue [1,2,3,6,7,*], Tingdi Chen [1,2,3,6] and Xiangkang Dou [1,6,7]

1 CAS Key Laboratory of Geospace Environment, Department of Geophysics and Planetary Sciences, University of Science and Technology of China, Hefei 230026, China
2 Mengcheng National Geophysical Observatory, School of Earth and Space Sciences, University of Science and Technology of China, Hefei 230026, China
3 CAS Center for Excellence in Comparative Planetology, Hefei 230026, China
4 Institute of Deep Space Sciences, Deep Space Exploration Laboratory, Hefei 230026, China
5 Key Laboratory of Geological Survey and Evaluation of Ministry of Education, China University of Geoscience, Wuhan 430074, China
6 Collaborative Innovation Center of Astronautical Science and Technology, Hefei 230026, China
7 Hefei National Laboratory, University of Science and Technology of China, Hefei 230088, China
* Correspondence: xuexh@ustc.edu.cn

Abstract: This study presents the observations of midlatitude plasma irregularities over Eastern Asia during a moderate magnetic storm on 16 July 2003. Multi-instrumental observations, including the ground-based ionosondes, the GNSS networks, and the CHAMP and ROCSAT-1 satellites, were utilized to investigate the occurrence and characteristics of midlatitude plasma irregularities. The midlatitude strong spread F (SSF) mainly occurred in the midnight–morning sector as observed by ionosondes over Japan during this storm. SSF was related to plasma depletions, which is also recorded by GNSS network in the form of the enhancement of the rate of total electron content (TEC) change index (ROTI). The possible mechanism for the generation of SSF is that the enhanced eastward electric fields, associated with the prompt penetration electric fields and disturbance dynamo electric fields, cause the uplift and latitudinal extension of equatorial plasma bubbles (EPBs) to generate the observed midlatitude SSF further. Meanwhile, plasma density increased significantly under the influence of this storm. In addition, other common type of spread F, frequency spread F (FSF), was observed over Japan on the non-storm day and/or at high latitude station WK545, which seems to be closely related to the coupling of medium-scale traveling ionospheric disturbances (MSTIDs) and sporadic E (Es) layer. The above results indicate that various types of midlatitude spread F can be produced by different physical mechanisms. It is found that SSF can significantly affect the performance of radio wave propagation compared with FSF. Our results show that space weather events have a significant influence on the day-to-day variability of the occurrence and characteristics of ionospheric F-region irregularities at midlatitudes.

Keywords: ionospheric F-region irregularity; spread F; midlatitude plasma depletions; magnetic storm; Eastern Asia

check for updates

Citation: Ye, H.; Yi, W.; Zhou, B.; Wu, J.; Yu, B.; Tian, P.; Wang, J.; Long, C.; Lu, M.; Xue, X.; et al. Multi-Instrumental Observations of Midlatitude Plasma Irregularities over Eastern Asia during a Moderate Magnetic Storm on 16 July 2003. *Remote Sens.* **2023**, *15*, 1160. https://doi.org/10.3390/rs15041160

Academic Editors: Chunhua Jiang, Huijun Le, Ercha Aa and Zheng Li

Received: 20 January 2023
Revised: 15 February 2023
Accepted: 17 February 2023
Published: 20 February 2023

1. Introduction

Ionospheric F-region irregularities, also called equatorial plasma bubbles (EPBs), refer to plasma density depletions with respect to the background ionosphere, and are generally regarded as nighttime phenomena occurring in the equatorial region within a narrow distribution of $\pm 20^\circ$ magnetic latitudes [1–4]. Booker and Wells [5] reported the first observation of ionospheric F-region irregularities, which appear as scattered echo traces in high-frequency band ionograms, a phenomenon known as spread F. It is generally accepted that the generalized Rayleigh–Taylor (RT) instability performs an important role in triggering EPBs after sunset [6–8]. The RT instability is excited in the bottom side F region, then evolves into plasma bubbles that penetrate the F peak to the topside F region [6–8]. Importantly, the growth of the RT instability can be modulated by several factors, such as the electric field, plasma density gradient, neutral wind, and gravity waves [8]. Therefore, the occurrence of EPBs shows significant seasonal, longitudinal, altitude, solar, and magnetic activity dependence [2,9–12]. EPBs are known to severely affect the performance of transionospheric radio waves, called ionospheric scintillation, leading to sharp fluctuations in the amplitude and phase of radio signals from satellite radio communication and navigation systems [12–15]. Therefore, it is of great importance to study the occurrence and characteristics of the ionospheric F-region irregularities under different ionospheric background conditions.

While ionospheric F-region irregularities are primarily confined in the equatorial region, large amplitude plasma depletions have occasionally been observed at midlatitudes [3,16–20]. For example, Ma and Maruyama [17] detected a super plasma bubble at 30°N magnetic latitudes by using dense GPS receivers. In European midlatitudes, plasma bubbles of equatorial origin have been observed through the dense GNSS networks and satellite in situ measurements [18,19]. Aa et al. [20] presented a case study of midlatitude plasma bubbles after sunset over China and adjacent areas during the main phase of a storm on 8 September 2017. In the American sector, Martinis et al. [21] found that midlatitude plasma bubbles can be identified in the form of airglow depletions. Huang et al. [8] reported that the highest latitude (altitude) of ionospheric F-region irregularities in the literature occurred at 46° magnetic latitudes and reached an apex altitude of 6800 km over the magnetic equator. Generally, two main mechanisms can be responsible for the formation of midlatitude plasma depletions. One reasonable interpretation is that midlatitude plasma depletions are the poleward extension of EPBs along the magnetic field lines under the additional eastward electric field. Typically, such eastward electric fields are considered to be the generated electric field (i.e., prompt penetration electric fields [PPEF] and/or disturbance dynamo electric fields [DDEF]) at high-latitude regions that penetrates to the equator and low latitudes during magnetic storms [20–24]. In addition, Rajesh et al. [25] recently proposed that the sunset eastward electric field intensified by the Tonga volcano-induced effects can also produce plasma bubbles poleward extending to middle latitudes in both hemispheres. The other explanation for the generation of midlatitude plasma depletions is in association with medium-scale traveling ionospheric disturbances (MSTIDs) characterized by wave-like structures in the midlatitude ionosphere [26–31]. By using all-sky airglow imagers, Sun et al. [26] found that the evolution of mesoscale field-aligned irregularity structures was strongly associated with the intensity of the main-body MSTIDs. Some studies have reported that the observations of midlatitude plasma depletion were associated with MSTIDs in the absence of EPBs signatures in the equatorial region during three different magnetic storms [4,16,30].

In addition to these two common mechanisms, it is also found that some driving factors can locally produce midlatitude plasma depletion, especially in the dayside ionosphere, when ionospheric F-region irregularities usually do not occur. Park et al. [32] investigated a dayside midlatitude plasma depletion without fine structures at altitudes near 430–520 km during quiet geomagnetic conditions, excluded the possibility of an equatorial depletion source, and believed that it may be related to gravity waves. In addition, unusual dayside midlatitude plasma depletions were detected a few hours after rocket launches, due to chemical recombination caused by exhaust plumes along the rocket's ascending trajectories [33]. Overall, the possible generation mechanisms of midlatitude plasma depletions are diverse and still not well understood, which is worthy of further investigation with more observations and events.

In this study, we present an intriguing case study of midlatitude plasma irregularities over Eastern Asia that occurred during a moderate magnetic storm on 16 July 2003. By jointly using multi-instrumental observations, we investigated the roles of

EPBs and MSTIDs in generating midlatitude plasma depletion. The results show the day-to-day variability of the occurrence and characteristics of ionospheric F-region irregularities. A detailed description of the data is included in Section 2, while the analysis results are presented in Section 3. Our discussions and conclusions are contained in Sections 4 and 5, respectively.

2. Data

In this study, measurements from ionosondes, the ground-based Global Navigation Satellite Systems (GNSS) network, and the CHAMP and ROCSAT-1 satellites are utilized to study the occurrence of midlatitude plasma depletions over Eastern Asia under the influence of the magnetic storm on 16 July 2003. The geophysical conditions during this storm are described by the solar wind velocity, interplanetary magnetic field (IMF) Bz component, au-roral electrojet (AE) index, and geomagnetic indices (i.e., SYM-H and Kp).

A meridional chain of ionosondes along the longitude of ~135°E over Japan can be used to identify spread F and obtain the F2 layer critical frequency (foF2) from ionograms. From middle latitudes to low latitudes, they are Wakkanai (WK545: 45.4°N, 141.7°E), Kokubunji (TO536: 35.7°N, 139.5°E), Yamagawa (YG431: 31.2°N, 130.6°E), and Okinawa (OK426: 26.7°N, 128.2°E). The detailed location information of ionosonde stations is given in Table 1. Manually scaled parameters (i.e., foF2) with 1 h intervals were kindly provided by the National Institute of Information and Communications Technology (NICT) in Japan. We also manually checked the ionospheric parameter foF2, which are in good agreement with the NICT results. Moreover, we manually identified spread F with a 1 h sampling interval. Note that the local time in our analysis refers to the Japanese Standard time (JST = UT + 9 h), where UT is universal time.

Table 1. Coordinates of ionosonde stations used in this study. Geomagnetic latitude are obtained from the International Geomagnetic Reference Field (IGRF)-2005 magnetic field model.

Station (Abbr.)	Geographic Latitude	Geographic Longitude	Geomagnetic Latitude
Wakkanai (WK545)	45.4°N	141.7°E	40.5°N
Kokubunji (TO536)	35.7°N	139.5°E	30.0°N
Yamagawa (YG431)	31.2°N	130.6°E	26.1°N
Okinawa (OK426)	26.7°N	128.2°E	21.2°N

Data derived from the ground-based GNSS network can help characterize ionospheric density and disturbances [34]. First, the total electron content (TEC) is calculated through multiple steps using the dual-frequency carrier phase and pseudorange, which can be found in the detailed work of previous work [35,36]. Then, the TEC was further processed to obtain the rate of TEC change index (ROTI) and the detrended TEC products. The ROTI is defined as the standard deviation of the rate of the TEC change over 5 min. Details of the method used to obtain the ROTI were described by Sori et al. [37]. Here, the two-dimensional global maps of ROTI indices, provided by the Institute for Space-Earth Environmental Research (ISEE) at Nagoya University, are used to detect the existence of ionospheric F-region irregularities on a global scale [38,39]. The detrended TEC products were produced by subtracting the background TEC using a 15 min running window [16]. In this study, the detrended TEC maps produced by the NICT are used to identify MSTIDs over Japan.

To detect EPBs over Eastern Asia, the ROCSAT-1 and CHAMP satellites are also included in this study. The ROCSAT-1 satellite is in a near-circular orbit at an altitude of ~600 km with a 35° inclination, which can provide the in situ ion density (Ni), and plasma drift at a sampling cadence of 1 s via the Ionospheric Plasma and Electrodynamics Instrument (IPEI) payload and the retarding potential analyzer (RPA) [1,40]. The CHAMP satellite is in a circular, near-polar orbit with an inclination of 87.3°, and an initial altitude of

450 km. The in situ electron density (Ne, equal to Ni) is measured by the Planar Langmuir Probe (PLP) with a 1-s sweep every 15 s on board CHAMP [41].

3. Results

The wide distribution of ground-based GNSS networks provides an opportunity for a global overview of the occurrence of ionospheric F-region irregularities. Figure 1 shows the two-dimensional global maps of the ROTI indices as a function of geographical longitude and latitude at 18 UT on 15, 16, and 17 July 2003. The color indicates the ROTI value within a range from 0.0 to 1.0. The spatial resolution of the maps is 0.25 × 0.25 degrees. We note that an enhancement of the ROTI appeared from the equator to middle latitudes over Eastern Asia at 18 UT on 16 July 2003 in the middle panel in Figure 1. The local time at 135° longitude is approximately 03 JST. This means that postmidnight ionospheric F-region irregularities were observed. However, no EPBs signatures were observed over this region at the same moment on 15 and 17 July 2003. Therefore, it is worth further exploring what caused the occurrence of ionospheric F-region irregularities on 16 July 2003, even extending to the midlatitudes where the ionospheric F-region irregularities are rarely detected. Another attractive feature in Figure 1 is that the enhancements of ROTI occurred in the high latitudes in both hemispheres during the three days. The high-latitude ionospheric F-region irregularities are produced by energetic particle precipitation from the Earth's magnetosphere and convective plasma processes [42,43], which is beyond the scope of this study.

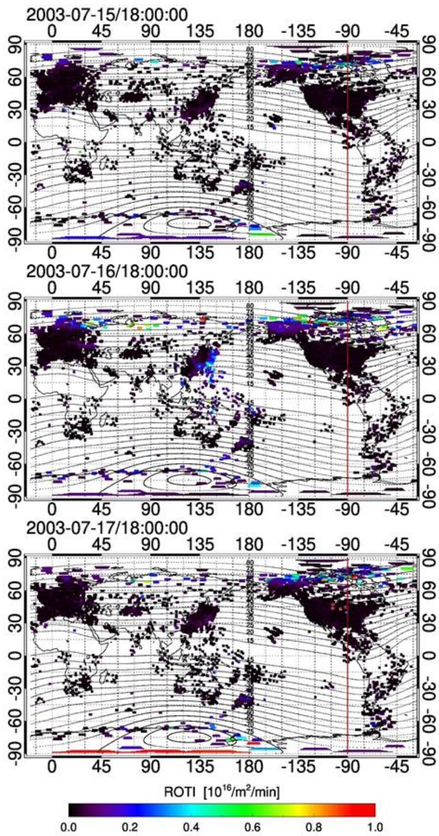

Figure 1. Two-dimensional global maps of ROTI indices in geographic coordinates at 18 UT on (**top**) 15, (**middle**) 16, and (**bottom**) 17 July 2003, as calculated from GNSS receivers (https://stdb2.isee.nagoya-u.ac.jp/GPS/GPS-TEC/ (accessed on 20 January 2023)). The color indicates the ROTI value within a range from 0.0 to 1.0. The red vertical lines represent 12 LT. The contours represent the geomagnetic latitude.

Figure 2 displays the geophysical conditions that occurred during the period 15–17 July 2003. The solar wind velocity in Figure 2a only increased from ~550 km/s to ~600 km/s. As shown in Figure 2b, the IMF Bz component sharply turned south at ~6 UT on 16 July, remained south for approximately 7 h, then slowly and continuously turned northward over a long period. At ~5 UT on 16 July, the IMF Bz component quickly turned southward for an hour, then northward. We also note that the IMF Bz component turned to the south and lasted for ~3 h at 10 UT on 15 July. In addition, the IMF Bz component also experienced large north–south fluctuations at other times. The increase in the AE index, shown in Figure 2c, indicated that several strong magnetospheric substorms occurred during the period of 15–17 July 2003. In particular, the substorm onset was related to the southward excursion of the IMF Bz component and the maximum value reached was at ~2 UT on 16 July (Figure 2c). At ~4 UT on 16 July 2003, the sudden decrease in the SYM-H index in Figure 2d indicated the start of the main phase of the magnetic storm. Eventually, the SYM-H index reached its minimum value of −100 nT at ~12 UT on 16 July 2003. After that, this moderately intense magnetic storm experienced a long recovery phase. The value of the Kp index slightly increased to more than 4 during the main phase, as shown in Figure 2e. Taken together, the above parameters in Figure 2 suggest that the PPEF and DDEF were produced on 16 July 2003 during this magnetic storm. Thus, the changed geophysical conditions may have been responsible for the enhancements in the ROTI over Eastern Asia on 16 July 2003 (Figure 1). More investigations are presented in the following text to illustrate the background ionosphere and possible physical processes.

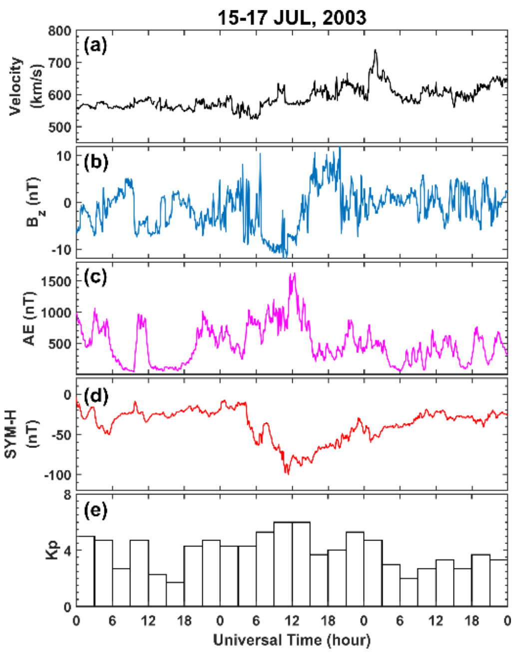

Figure 2. Geophysical conditions during the period 15–17 July 2003: (**a**) solar wind velocity, (**b**) IMF Bz, (**c**) AE index, (**d**) SYM-H index, and (**e**) Kp index. IMF = interplanetary magnetic field.

Figure 3 displays the SYM-H and IMF Bz indices, and the variation in foF2 observed by a meridional chain of four ionosondes along the longitude of ~135°E with decreasing latitude during the period 15–17 July 2003. The blue lines with stars represent the foF2 parameter. For comparison, the gray lines indicate the 27 day moving average value of foF2. On 16 July, Figure 3a shows the geomagnetic storm development during the period 15–17 July 2003. Figure 3c–e show that the first obvious increase peak of foF2 appeared at 5 UT on 16 July 2003, when the IMF Bz rapidly turned southward. The southward IMF Bz usually produced the eastward PPEF in the equatorial daytime ionosphere. It is likely that the enhanced eastward electric field causes an equatorial fountain effect, transporting plasma from the equatorial region to higher altitudes and latitudes [44]. However, at the higher latitude WK545 station, no enhancement of foF2 was observed at the same moment as shown in Figure 3b, suggesting that the range of latitudes affected by this PPEF was limited. After that, Figure 3b–e show that foF2 started to increase at ~7–9 UT with a large amplitude compared with that on the reference day, showing a positive storm effect. It seems that the foF2 started to increase first at the lower latitude station, especially in Figure 3c–e. The enhancements of foF2 lasted for more than 10 h from the main phase to the recovery phase of this storm. Then, the decrease in foF2 occurred at ~1 UT on 17 July, and this negative storm effect lasted for almost the entire day. Figure 4b–e also present the existence of spread F marked as light purple stars, as recorded by ionograms with 1 h intervals. Here, we did not distinguish the types of spread F. To our surprise, spread F signatures were observed at all four ionosondes every night during the period 15–17 July 2003. After storm onset, Figure 3b–e show that the durations of spread F at WK545, TO536, YG431, and OK426 were 14–21 UT (23-06 JST), 19–23 UT (04-07 JST), 18–24 UT (03-08 JST), and 14–22 UT (23-06 JST) on 16 July, respectively. Spread F at WK545 and OK426 occurred slightly earlier than midnight, while spread F at TO536 and YG431 occurred after midnight. The above spread F tended to occur at 18–24 UT (03-08 JST), which is persisted until the next morning. On 15 and 17 July, spread F tended to mainly occur at 12–18 UT (21-03 JST) and remained continuous, except for the occurrence at YG431 and OK426 where the duration of spread F was not completely continuous on 15 July. Although few spread F lasted into the morning, such as at OK426 on 15 July, they disappeared no later than 06 JST, and slightly earlier than that on 16 July.

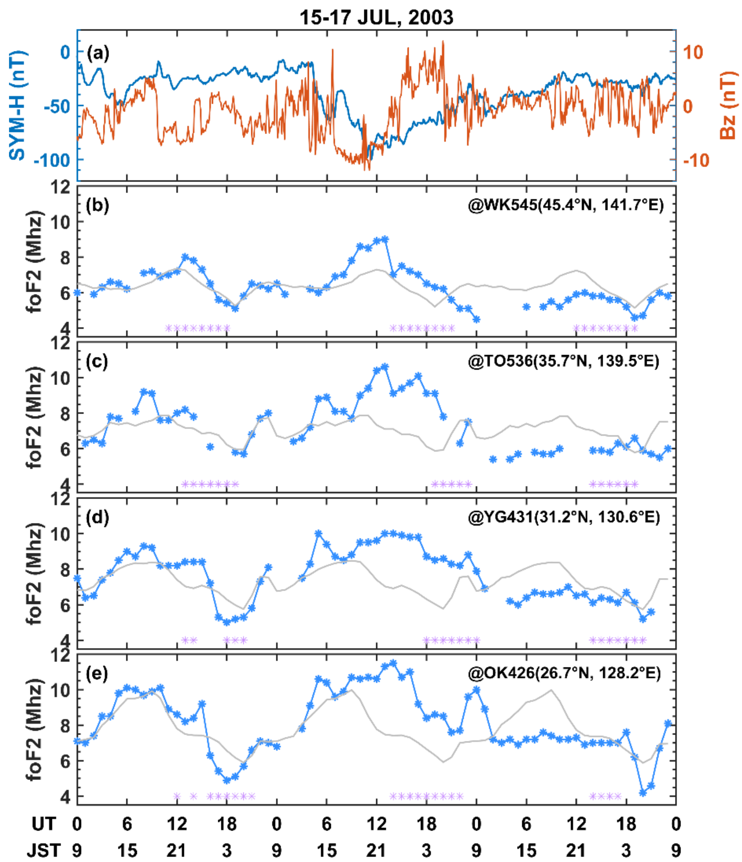

Figure 3. (**a**) The SYM-H (blue line) and IMF Bz (orange line) indices show geomagnetic storm development during the period 15–17 July 2003. Variations in the F2 layer critical frequency (foF2) at (**b**) WK545, (**c**) TO536, (**d**) YG431, and (**e**) OK426 during the period of 15–17 July 2003, as measured by ionosonde. Gray lines represent the 27-day moving average value as a reference. The light purple stars indicate the spread F obtained from ionograms. Note that JST = UT + 9.

To facilitate the study of the evolution and occurrence characteristics of spread F, we further present ionograms with 1 h intervals. Usually, spread F is identified as four types: frequency spread F (FSF), range spread F (RSF), mixed spread F (MSF), and strong range spread F (SSF) [45–47]. FSF in the ionograms appears as the intensity of scattered echo traces increased with frequency, accompanied by the failure to identify foF2. RSF is scattered echo traces at lower frequency with clear foF2. MSF is a mixture of FSF and RSF. SSF is described as an extended range spread on F region echoes traces that significantly extend beyond the local foF2 value [45]. Combined with the statistical results in Figure 3, Figure 4 first illustrates the evolution of spread F at four ionosondes during the period 17–22 UT (02-07 JST) on 16 July 2003. At first glance, the occurrences of spread F were indeed quite high during this period of interest. Especially at the three lower latitude stations of TO536, YG431, and OK426, we notice that the scattered echo traces are mainly SSF, as shown in Figure 4. It seems that the lower the latitude of the station is, the earlier the time of SSF appears. On the top panel (WK545) in Figure 4, the SSF that occurred at 17–19 UT (02-04 JST) is not as strong as spread F at the three lower latitude stations. At 20–21 UT, the types of spread F changed to weak FSF. The different morphology of spread F traces suggested that the generation mechanism of spread F at WK545 may be different from that at other stations. In addition, Figure 4 also presents the high-frequency occurrence of sporadic E (Es) with a relatively small magnitude at altitudes of ~100 km. Intriguingly, the so-called cusp type Es, which is connected to the thick E layer trace [29], developed well in the ionospheric E region after 21 UT (06 JST) during the local morning.

To uncover the possible difference in the occurrence and characteristics of spread F before and after the storm onset, we first investigate the ionosonde observations on 15 July 2003. Since the occurrence of spread F on 15 July was preferentially concentrated at 12–18 UT (21-03 JST) as shown in Figure 3, the period 11–16 UT (20-01 JST) was selected to show the evolution of spread F. The observed spread F was mainly FSF in Figure 5 during the period 11–16 UT on 15 July. We note that satellite traces, appearing as one or more quasi replicas of the F layer trace [47–49], are clearly seen from 12 UT to 16 UT at To536. In other subgraphs of Figure 4, for example, clear satellite traces can be seen near the second hop at 15 UT (24 JST) at WK545, YG431, and OK426. Tsunoda [49] and Li et al. [50] also observed the satellite trace near the second hop. Interestingly, some of the observed morphology of FSF, for example at 12 UT (21 JST) at OK426, was similar to the daytime spread F observed by Jiang et al. [47]. In addition, we note that flat type Es can be seen in almost every ionogram, showing a wide distribution of Es over Japan on 15 July. It should be mentioned that the existence of Es may affect the observation of the ionospheric F region to some extent. As a comparison with Figure 5, we represent the development of spread F in Figure 6 during the same UT period, but on 16 July, when the magnetic storm occurred, to further study the possible difference. The echo traces in Figure 6 show that the occurrence of spread F is obviously reduced and mostly replaced by the normal F region trace. At the lowest latitude station of OK426, spread F started to be FSF at 14 UT, then developed into SSF at 15–16 UT. At the highest latitude station of WK545, the type of spread F during the period 14–16 UT is MSF, accompanied by obvious satellite traces. In Figure 6, flat type Es can still be identified, but the magnitude is weaker than that observed in Figure 5. The results from Figures 4–6 suggest that the occurrence time and type of spread F caused by storms are significantly different from those generated during non-storm periods. It also suggests that the generation mechanism should be somewhat different.

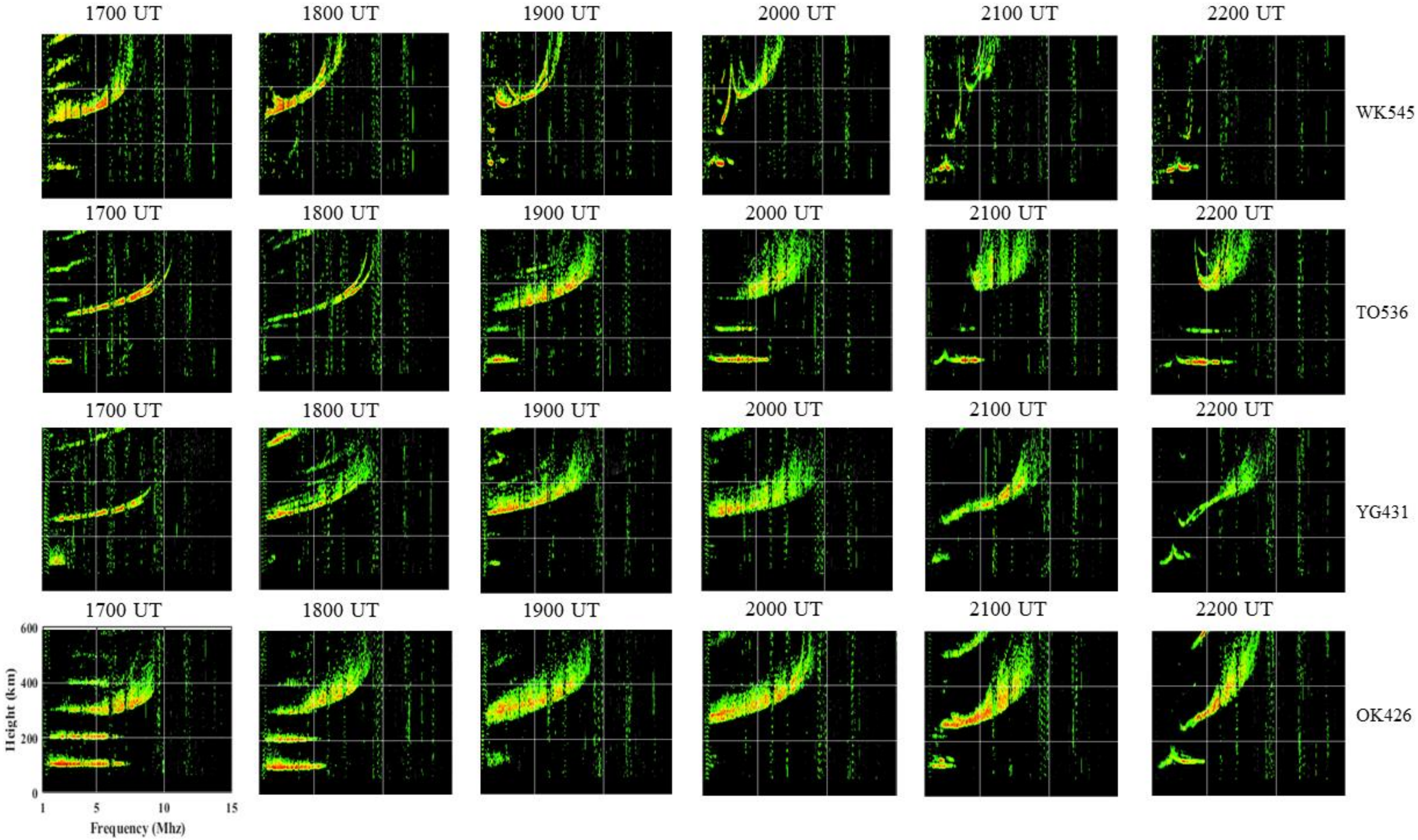

Figure 4. Development of spread F at (**top panel**) WK545, (**second panel**) TO536, (**third panel**) YG431, and (**bottom panel**) OK426 during 17–22 UT (02-07 JST) on 16 July 2003. Coordinate reference information is given in the lower left figure.

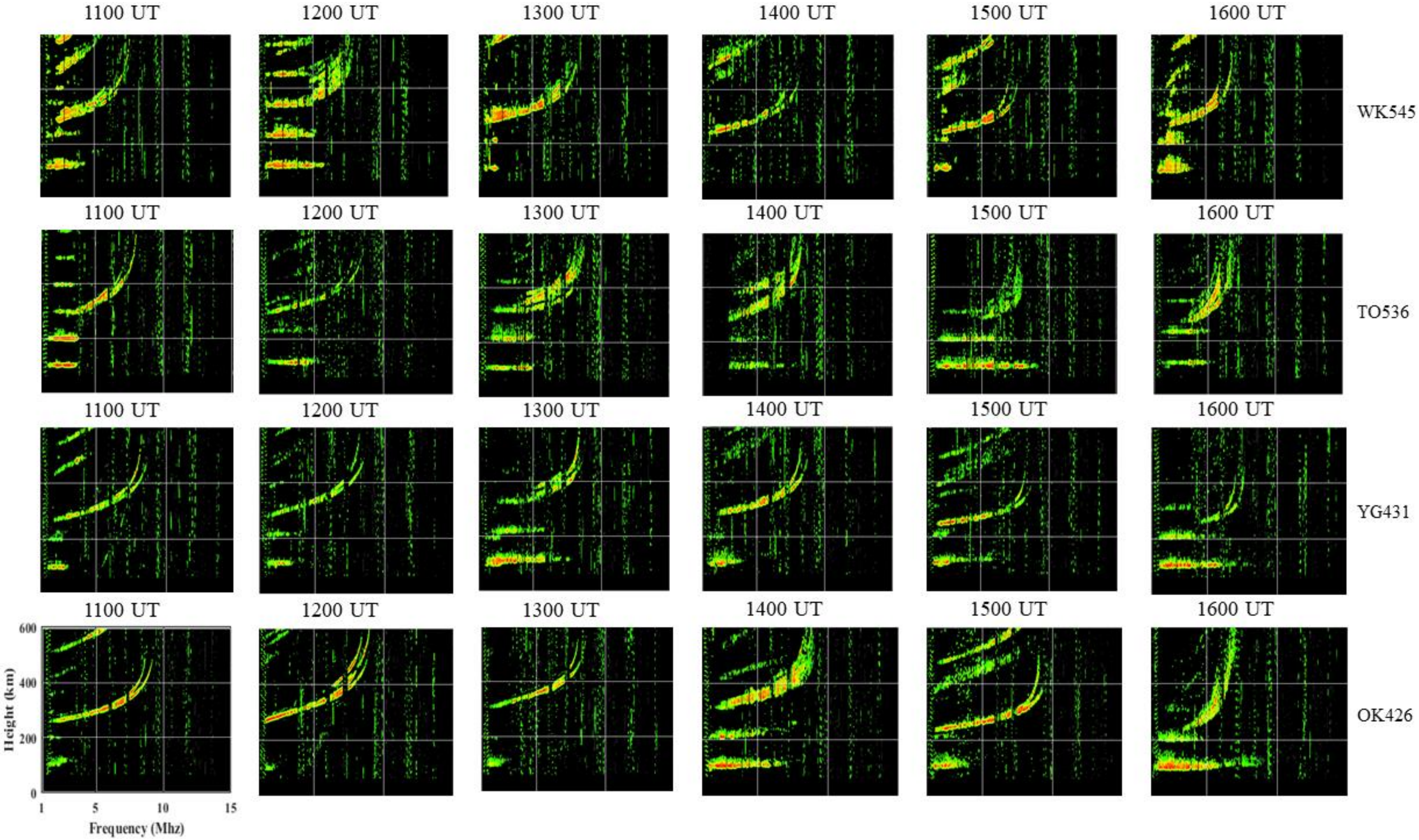

Figure 5. Development of spread F at (**top panel**) WK545, (**second panel**) TO536, (**third panel**) YG431, and (**bottom panel**) OK426 during 11–16 UT (20-01 JST) on 15 July 2003. Coordinate reference information is given in the lower left figure. ordinate reference information is given in the lower left figure.

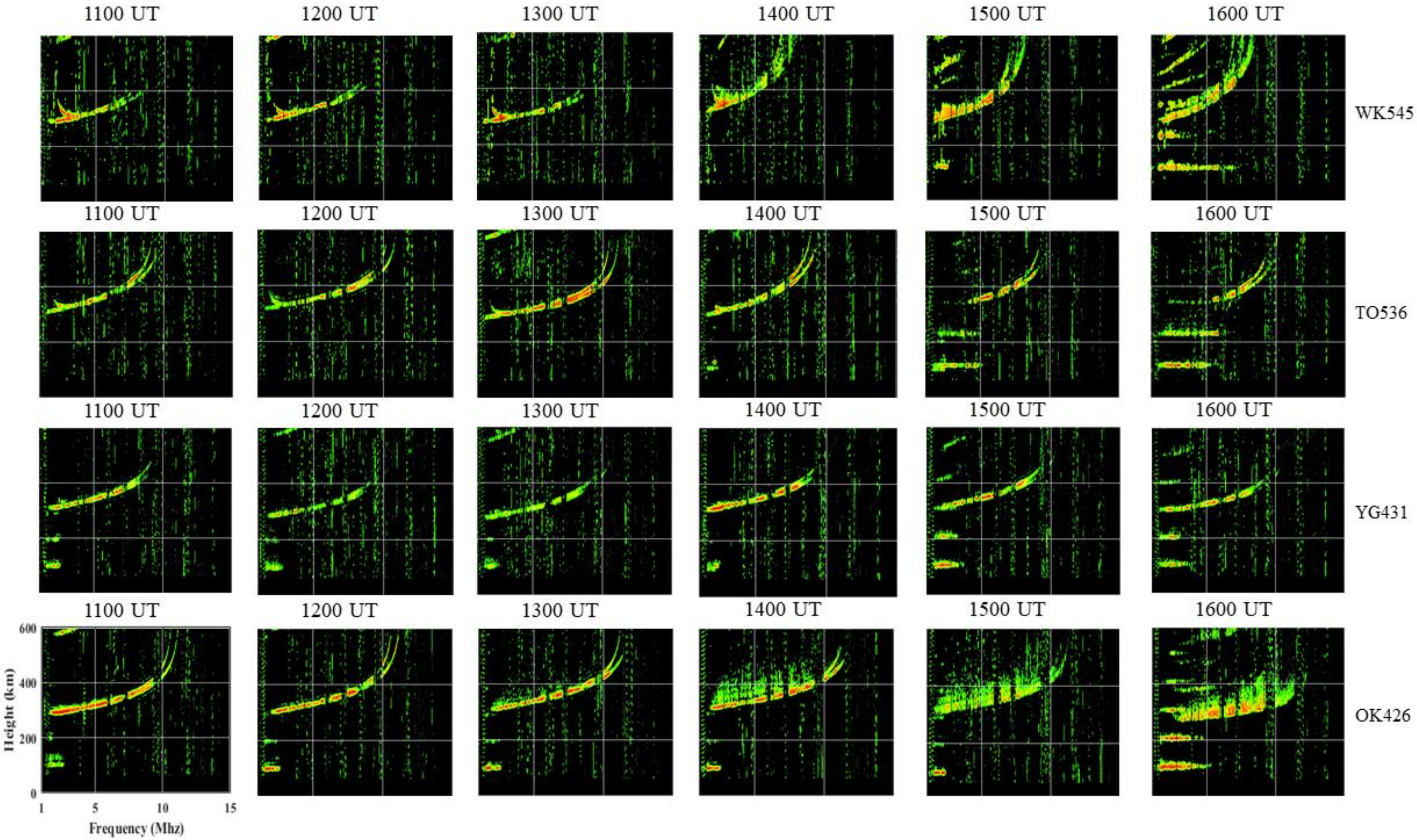

Figure 6. Development of spread F at (**top panel**) WK545, (**second panel**) TO536, (**third panel**) YG431, and (**bottom panel**) OK426 during 11–16 UT (20-01 JST) on 16 July 2003. Coordinate reference information is given in the lower left figure.

Figure 7 displays the multiple satellite ascending tracks of ROCSAT-1 and the corresponding density irregularity structure detected over Eastern Asia during the period 13–24 UT on 15, 16, and 17 July. The tracks were marked with the corresponding labels. The purple stars along the ROCSAT-1 orbits represent each of the identified density irregularity structures (the criterion of σ ≥ 0.3%), determined by the calculation from the method proposed by Su et al. [1]. The red dots represent the geographic location of the four ionosondes (WK545, TO536, YG431 and OK426) used in this study. As seen in Figure 7b, from the magnetic equator to midlatitudes, a large number of density irregularity structures were detected by ROCSAT-1 on tracks b1–b7, indicating a strong disturbance in the nighttime ionosphere over Eastern Asia. The observation of density irregularity structure in ROCSAT-1 tracks over Japan can be associated with spread F observed in ionograms during the same period, as shown in Figure 4. Significantly, ROCSAT-1 detected a few density irregularity structures on 15 and 17 July as shown in Figure 7a,c, which are consistent with the observations in Figure 1a,c. On 15 July, Figure 7a shows that the density irregularity structure mainly occurred near the magnetic equator of tracks a5 and a6. On 17 July, Figure 7c displays that the density irregularity structures were mainly scattered on track c7. Thus, combined with the results of Figure 7a,c, the observation in Figure 7b indicated that magnetic storms should perform an important role in the formation of the density irregularity structure over Eastern Asia.

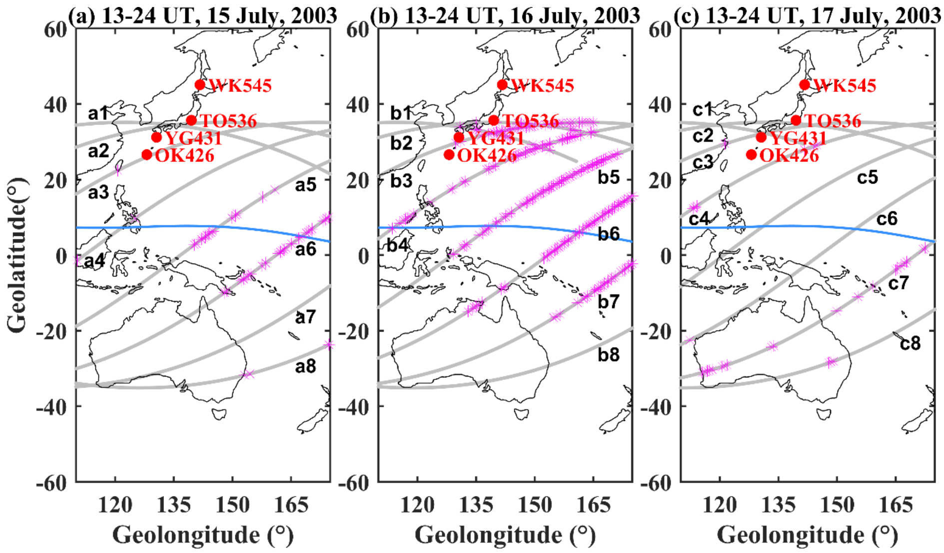

Figure 7. ROCSAT-1 ascending tracks marked with different labels over the Eastern Asian sector during 13–24 UT on (**a**) 15, (**b**) 16, and (**c**) 17 July 2003. The purple stars along the ROCSAT-1 orbits represent each of the identified density irregularity structures (the criterion of σ ≥ 0.3%) obtained from the method proposed by Su et al. [1]. The red dots represent the geographic location of the four ionosondes (WK545, TO536, YG431, and OK426 used in this study). The blue lines indicate the geomagnetic equator.

In order to more directly identify plasma density depletion, Figure 8 further shows the variation in in situ ion density measured by ROCSAT-1 as a function of geographic longitude with its tracks corresponding to the marks in Figure 7. The UT time is drawn in the upper right corner of each subfigure. Figure 8 shows that compared with the plasma density on 15 and 17 July, the overall plasma density on 16 July was obviously enhanced, consistent with the enhancements of foF2 observed during the magnetic storm in Figure 3. In addition, Figure 8a,c show relatively stable changes in plasma density. However, Figure 8b shows that ROCSAT-1 encountered clear plasma density depletion on tracks b1–b7, proving the reliability of the density irregularity structure identified in Figure 7b. It should be noted that this plasma depletion mainly occurred in the midnight-morning sector. No signatures of plasma depletion were measured on track b8, which may be due to the time required for EPBs to grow from the magnetic equator to southern midlatitudes. We note in Figure 8b that the eastern edge of plasma density depletion moved westward as time passed, especially from tracks b5 to b1. We checked the westward drift motion of plasma depletion on the zonal drift parameters recorded by ROCAST-1. After 22 UT, only small magnitudes of plasma density depletions were detected around the latitude of Japan on tracks b1 and b2. This is because after dawn, the photoionization process can produce new plasma particles to fill plasma depletion at high altitudes. As shown in Figure 8b, other ionospheric irregularity structures, i.e., plasma blobs, appear in the form of plasma density enhancement around the longitude of ~135°/~160° on tracks b6/b7, respectively. These plasma blobs on both tracks also identified at similar latitudes in the Southern Hemisphere as suggested in Figure 7, indicating a possible linkage of the extension of EPBs [51,52]. Figure 8a shows a series of weak plasma depletions on tracks a5 and a6, corresponding to the density irregularity structure recorded near the magnetic equator in Figure 7a. We inferred that these weak plasma depletions were the remnant of the EPBs initiated during sunset hours. Some of plasma density enhancements shown in Figure 8c were also identified as ionospheric irregularity structures in Figure 7c. The detailed generation mechanism of plasma density enhancement is beyond the scope of this study.

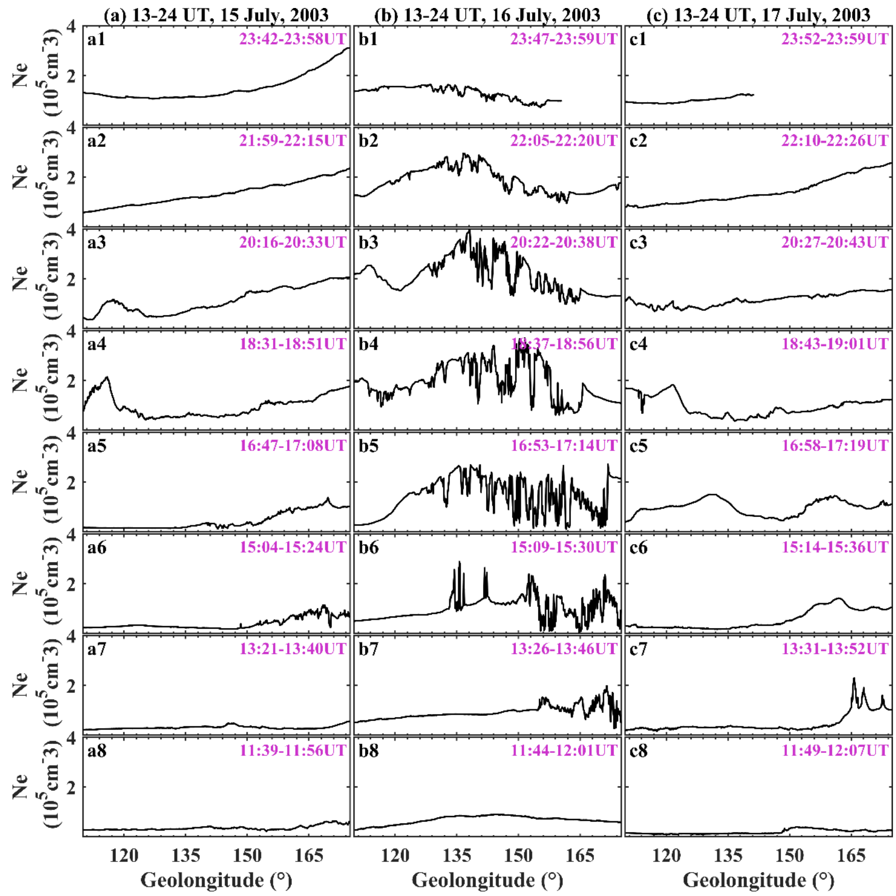

Figure 8. ROCSAT-1 observations of in situ ion density (Ni) variation as a function of geographic longitude over the Eastern Asian sector during 13–24 UT on (**a**) 15, (**b**) 16, and (**c**) 17 July 2003. The corresponding labels are the same as those used in Figure 7. Universal time (UT) information is given in the upper right corner of each subfigure.

To study the behavior and evolution of plasma depletion, Figure 9 shows the variation in the 5-s averaged plasma vertical and zonal drifts for the corresponding ROCSAT-1 tracks as shown in Figure 8b. The UT time is drawn in the bottom right corner of each subfigure. Many wave-like variations exist in plasma drift especially in zonal drift on some tracks, such as b1–b4, which is due to the influence of solar photons on RPA after sunrise [53]. In addition, some outliers were also occasionally recorded by ROCSAT-1.

Therefore, we need to try our best to recognize the feature of drift inside plasma depletion and reveal some disturbance effects caused by magnetic storm. Figure 9a shows that the vertical drifts inside plasma depletions were upward with the magnitude of over 100 m/s on tracks b5–b7 in the postmidnight sector. This upward drift indicated the continuous growth and extension of plasma depletion, suggesting that plasma depletion is still alive during that postmidnight period. Another important feature in Figure 9a is that the vertical drift has a weak upward velocity in the ambient ionosphere on most tracks, as opposed to the downward plasma velocity during quiet-time periods. The upward drift moves plasma from a lower altitude to a higher altitude, causing an uplift of the ionospheric F region [51,53,54]. Since plasma resides at higher altitudes where the recombination rate is low, the enhancements in foF2 and in situ ion density were observed by ionosondes and ROCSAT-1, respectively. Importantly, owing to the lower recombination rate at high altitudes, the strong uplift of the ionosphere is more conducive to EPBs generation due to the high RT instability growth rate. Moreover, such ionospheric conditions also become more favorable to the existence of long-lasting plasma bubbles because it should take a long time for the photoionization process to produce enough new plasma particles to refill the low-density region at high altitudes [51,54]. During the quiet-time period, the nighttime zonal drifts were eastward, and reversed its direction westward at ~05 LT as measured by the C/NOFS satellite [55]. However, the ambient zonal drifts were westward in the midnight-morning sector observed during this storm as shown in Figure 9b. In particular, zonal drifts inside plasma depletion on tracks b5 and b6 were strongly westward. The above results suggested that plasma drifts in the ambient ionosphere were strongly affected by the magnetic storm.

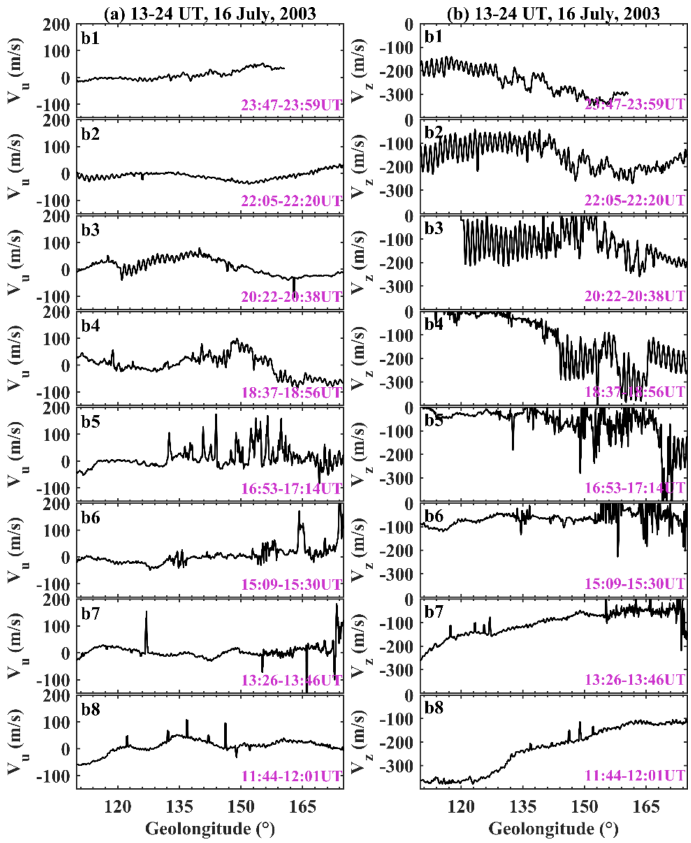

Figure 9. ROCSAT-1 observations of 5-s averaged plasma (**a**) vertical and (**b**) zonal drift variation as a function of geographic longitude over the Eastern Asian sector during 13–24 UT on 16 July 2003. The orbits are the same as those used in Figure 7b. Universal time (UT) information is given in the lower right corner of each subfigure.

Figure 10 presents the CHAMP descending tracks and the corresponding in situ electron density over Eastern Asia during the period 11–15 UT on 15–17 July 2003. The tracks are colored differently to indicate the corresponding date. Similar to Figure 7, the red dots represent the geographic locations of the four ionosondes used in this study. Due to the high inclination of CHAMP, the local time of descending tracks has little change during the three days [55], which is approximately at a fixed local time near 2230 LT. We plotted the measured electron density in Figure 10b–g, respectively, following the orbital arrangement from west to east in Figure 10a. To be convenient for comparison, we adjusted the position of the corresponding tracks in Figure 10d,e. The date marked with the corresponding color is drawn in the bottom right corner of each subfigure. The most prominent feature is the wide and deep plasma depletion that was clearly seen symmetrically at the magnetic equator in Figure 10c,f on 16 July. As shown in Figure 10f, the latitudinal coverage even reached ~30°N over the two lower latitude ionosondes in Japan. The relatively small latitudinal extension of plasma depletion in Figure 10c reveals the possible reason why plasma depletion was not observed at the crossed longitude on track b7 of ROCAST-1 in Figure 8b at the same time. At 14 UT (23 JST) on 16 July, the only observation of spread F at OK426 of the four stations in Figure 6 might be associated with the northern edge of plasma depletion on the track of CHAMP in Figure 10c. On 15 and 17 July, we note that no signatures of plasma depletion were detected by CHAMP, which may explain why no enhancement of ROTI was observed later hours in Figure 1a,c. Due to the gradual decay of the ionosphere after sunset [53], a single equatorial anomaly crest appeared over the magnetic equator on 15 and 17 July. Notably, the overall ambient electron density detected by CHAMP was indeed enhanced as expected on 16 July. The observations of CHAMP further suggested that the magnetic storm had an important effect on the variations in the ionosphere and the generation of plasma depletion related to EPBs.

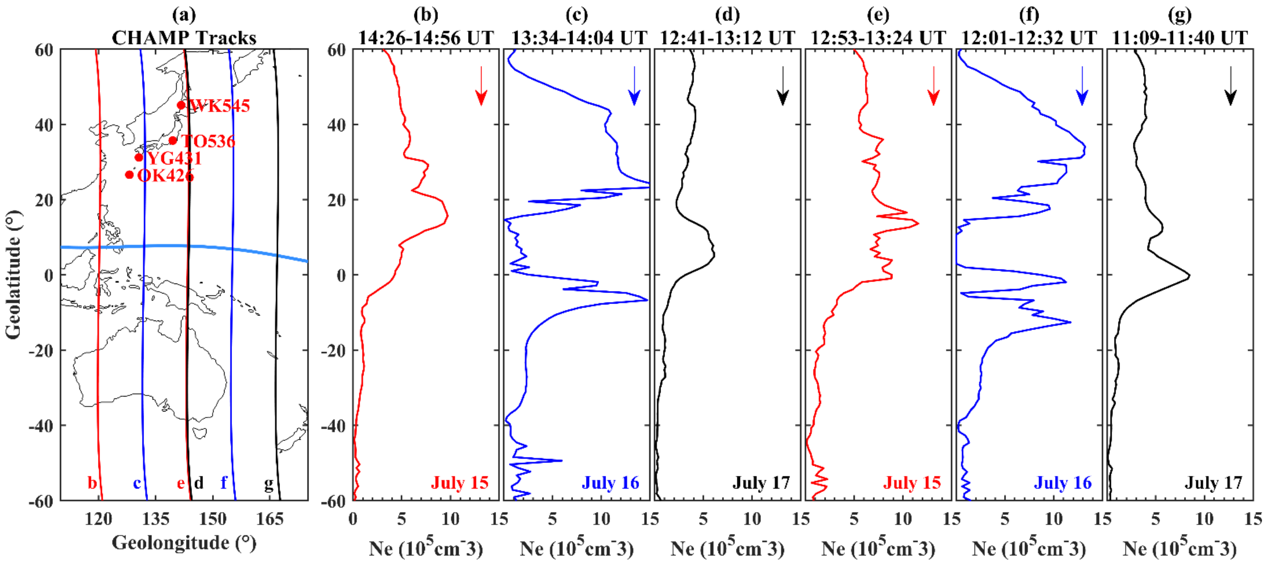

Figure 10. (**a**) CHAMP descending tracks marked with the corresponding right subgraph labels over the Eastern Asian sector during 11–15 UT on 15 (red), 16 (blue), and 17 (black) July 2003. The red dots represent the geographic location of the four ionosondes (WK545, TO536, YG431, and OK426 used in this study). The blue lines indicate the geomagnetic equator. The corresponding in situ electron density (Ne) variations as a function of geographic latitude are shown in right panels (**b**–**g**), respectively. The arrows indicate the descending orbits.

4. Discussion

Using multi-instrumental observations, this study reports an interesting case study of midlatitude plasma depletions over Eastern Asia that occurred during a moderate magnetic storm on 16 July 2003. These depletions are widely distributed in latitudes, even extending to midlatitudes over Eastern Asia, as detected by the in situ plasma density measured by ROCSAT-1 and CHAMP. Correspondingly, SSFs are recorded in the ionograms at three lower latitude stations over Japan on 16 July 2003, as shown in Figure 4. Generally, SSFs are thought to be related to ionospheric scintillation [45,46]. Thus, it is reasonable to infer that the enhancement of ROTI observed in Figure 1 is associated with SSF and depletions during this magnetic storm. Although no obvious signatures of plasma depletions were detected by satellites and GPS on 15 and 17 July 2003, FSF was still observed in the ionograms at multiple stations over Japan. In addition, it can be seen from Figure 4 that the types of spread F are mainly FSF at higher latitude station WK545, which is significantly different from that at the three lower latitude stations of TO536, YG431, and OK426. This implies that these two types of midlatitude spread F observed by ionosonde are possibly produced by the different physical mechanisms in our case.

The midlatitude plasma depletions observed during this magnetic storm are mainly centered in the midnight-morning sector, accompanied by an increase in plasma density. We note that the IMF Bz turned northward during this period, indicating an eastward penetration electric field caused by the over-shielding electric field in the nighttime ionosphere [22]. Simultaneously, the significant westward drift of plasma was confirmed by the observations of ROCSAT-1 in Figure 9b. Therefore, the expected DDEF could be produced by the thermospheric disturbance westward winds during the recovery phase of the storm [22–24]. DDEF is usually eastward (westward) in the nighttime (daytime) ionosphere. These superimposed eastward electric fields moved the F region plasma upward as observed by ROCSAT-1 in Figure 9a, which is conducive to the growth of the RT instability, and hence, results in favorable conditions for the generation and latitudinal extension of EPBs [7,19,20,50]. As a result of the extension of EPBs along the magnetic field lines, plasma blobs that occurred at low latitudes in the Southern Hemisphere were identified by ROCSAT-1 on tracks b6/b7. Eventually, midlatitude SSF related to the extension of EPBs was recorded in ionograms over Japan during this storm. In addition, we also note in Figure 4 that the lower the latitude of the ionosonde station is, the earlier the time of SSF appears. This characteristic suggests that the midlatitude SSF that occurred during this storm is not related to the enhanced activity of traveling ionospheric disturbances caused by Joule heating at auroral regions [19,20]. In addition, the enhanced eastward electric field may transport plasma from the equatorial region to higher latitudes [19,30], causing the enhancement of plasma density during this storm as observed by satellites and ionosondes.

As for FSF observed in ionograms, it may be induced by other physical processes. As shown in Figure 5, the signatures of the Es layer can be seen almost every ionogram. At the same time, a high occurrence of FSF was recorded by the four ionosondes in Japan. Additionally, we noticed in Figure 4 that there is an existence of a weak Es layer when FSF appears at WK545. According to previous studies [19,30,56,57], the midlatitude spread F may be associated with the coupling of Es layer and Perkins instability. It should be pointed out that Perkins instability is considered to be an important source of the generation of nighttime MSTIDs [57,58]. Furthermore, the Es layer, presented as thin-layered structures at altitudes of 90–130 km, facilitates the performance of Perkins instability [57–60]. Thus, we further investigated the possible mechanism. Figure 11 shows the two-dimensional maps of the detrended total electron content (TEC) over Japan at 13 UT (22 JST), 14 UT (23 JST), and 15 UT (24 JST) on 15 July 2003. We note that the periodic wave-like disturbances are clearly seen in the detrended TEC maps. Interestingly, the TEC wave fronts stretched from northwest to southeast, which is in good agreement with the normal propagation pattern under quiet magnetic conditions [31,58]. As shown in Figure 5, satellite traces observed in ionograms can also be considered indicators of large-scale waves in the nighttime ionosphere [49]. When we relooked at the plasma density measured by CHAMP, it was found in Figure 10b that wave-like structures with small magnitude appeared at 40°N at approximately 1430 UT, indicating the possible existence of MSTIDs. Moreover, we also note the presence of wave-like perturbations in other satellite tracks over Japan on 15 and 17 July 2003. Thus, it is reasonable to infer that the FSF observed in our case may be the manifestation of the coupling of MSTIDs and the Es layer. However, it does not provide conclusive evidence that needs to be studied further in future works.

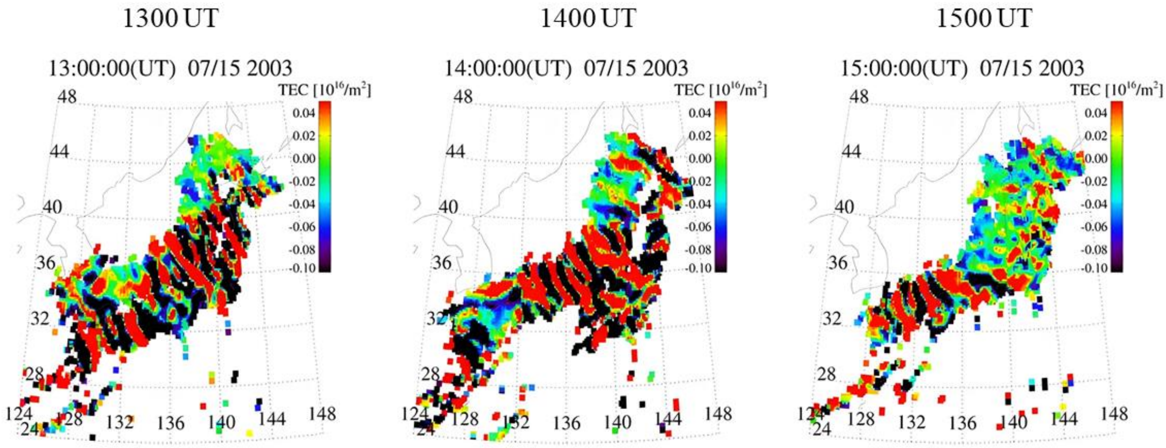

Figure 11. Detrended total electron content (TEC) maps over Japan (https://aer-nc-web.nict.go.jp/GPS/GEONET/ (accessed on 20 January 2023)) from 13 to 15 UT on 15 July 2003. The detrended TEC maps are obtained using a 15 min running window.

5. Conclusions

In this study, we have analyzed and presented the multi-instrumental observations of midlatitude plasma irregularities over Eastern Asia that occurred during a moderate magnetic storm on 16 July 2003. Through a global view of GNSS ROTI, we found that ionospheric F-region irregularities were observed from the equator to middle latitudes over Eastern Asia at 18 UT on 16 July 2003. It is further found that midlatitude SSF, lasting for several hours, mainly occurred in the midnight–morning sector over Japan during this storm. During the recovery phase of this storm, DDEF induced by the thermospheric disturbance winds and PPEF caused by the over-shielding electric field work together to be responsible for the enhanced eastward electric field and hence cause the uplift and latitudinal extension of EPBs to further generate the observed SSF and the enhancement of ROTI at midlatitudes. On the other hand, plasma density increased significantly during this storm compared with that on the reference day, because the plasma was transported from the equatorial region to higher latitudes. In addition to SSF observed during this storm, other common type of spread F, FSF, was observed in the Japanese sector on the reference day and/or at high latitude station WK545, which seems to be closely related to the coupling of MSTIDs and the Es layer. The above results indicate that various types of midlatitude spread F can be generated by different physical processes, showing the complicated day-to-day variability of the occurrence and characteristics of ionospheric F-region irregularities at midlatitudes. Significantly, we note that only midlatitude SSF related to the extension of EPBs, identified as clear plasma depletions by the satellites during this storm, can obviously affect the performance of the GNSS receiver as shown in Figure 1. More cases and numerical simulations are needed for further investigation and confirmation. Overall, the above results emphasize the effects of magnetic storm on the generation and evolution of midlatitude plasma irregularities. It is suggested that more research and attention should be given to midlatitude plasma irregularities in future studies.

Author Contributions: Conceptualization, H.Y., W.Y., J.W. (Jianfei Wu) and X.X.; methodology, H.Y. and X.X.; software, B.Z.; validation, J.W. (Jianyuan Wang) and C.L.; investigation, B.Y. and X.X.; data curation, P.T., C.L. and M.L.; writing—original draft preparation, H.Y.; writing—review and editing, W.Y., J.W. (Jianfei Wu), B.Y. and X.X.; visualization, H.Y. and B.Z.; supervision, X.X.; project administration, T.C.; funding acquisition, X.X. and X.D. All authors have read and agreed to the published version of the manuscript.

Funding: This work was supported by the National Key R\&D Program of China (Grant No. 2022YFF0503703), the National Natural Science Foundation of China (42188101, 42125402, 42074181, 42174183), the Project of Stable Support for Youth Team in Basic Research Field, CAS (YSBR-018), and the B-type Strategic Priority Program of CAS Grant No. XDB41000000. W.Y. was also funded by the Fundamental Research Funds for the Central Universities (grant No. YD3420002004), the Anhui Provincial Natural Science Foundation (grant No. 2008085MD113), and the Joint Open Fund of Mengcheng National Geophysical Observatory (MENGO-202209). J. Wu. was funded by the foundation of the National Key Laboratory of Electromagnetic Environment, and the Fundamental Research Funds for the Central Universities. B.Y. was funded by the Joint Open Fund of Mengcheng National Geophysical Observatory (Grant No. MENGO-202207).

Data Availability Statement: The ionosonde data are provided by the National Institute of Information and Communications Technology (NICT) at the ionosonde database website (https://wdc.nict.go.jp/IONO/HP2009/ISDJ/index-E.html (accessed on 20 January 2023)). The two-dimensional global maps of ROTI indices are available on the website of the Institute for Space-Earth Environmental Research (ISEE) at Nagoya University (https://stdb2.isee.nagoya-u.ac.jp/GPS/GPS-TEC/ (accessed on 20 January 2023)). The detrended TEC maps are provided on the NICT Dense Regional and Worldwide International GNSS-TEC observation (DRAWING-TEC) website (https://aer-nc-web.nict.go.jp/GPS/DRAWING-TEC/ (accessed on 20 January 2023)). The ROCSAT-1 satellite data can be downloaded from NCU (http://sdbweb.ss.ncu.edu.tw/v2/public/ (accessed on 20 January 2023)). The CHAMP satellite data are obtained from the Information System and Data Center (ISDC) of GFZ German Research Centre for Geosciences (http://isdc.gfz-potsdam.de (accessed on 20 January 2023)). The IMF data are available from NASA/GSFC's Space Physics Data Facility's OMNIWeb service (https://omniweb.gsfc.nasa.gov/ow_min.html (accessed on 20 January 2023)). The Kp index is obtained from the Center for Space Standards and Innovation (http://www.celestrak.com/SpaceData/ (accessed on 20 January 2023)).

Acknowledgments: The authors gratefully acknowledge the data providers for providing these data. The authors sincerely thank Yang-Yi Sun for his continued support and constructive discussion.

Conflicts of Interest: The authors declare no conflict of interest.

References

1. Su, S.Y.; Liu, C.H.; Ho, H.H.; Chao, C.K. Distribution characteristics of topside ionospheric density irregularities: Equatorial versus midlatitude regions. *J. Geophys. Res. Sp. Phys.* **2006**, *111*, A06305. [CrossRef]
2. Woodman, R.F. Spread F—An old equatorial aeronomy problem finally resolved? *Ann. Geophys.* **2009**, *27*, 1915–1934. [CrossRef]
3. Yu, T.; Ye, H.; Liu, H.; Xia, C.; Zuo, X.; Yan, X.; Yang, N.; Sun, Y.; Zhao, B. Ionospheric *F* layer scintillation weakening as observed by COSMIC/FORMOSAT-3 during the major sudden stratospheric warming in January 2013. *J. Geophys. Res. Sp. Phys.* **2020**, *125*, e2019JA027721. [CrossRef]
4. Kil, H.; Chang, H.; Lee, W.K.; Paxton, L.J.; Sun, A.K.; Lee, J. The origin of midlatitude plasma depletions detected during the 12 February 2000 and 29 October 2003 geomagnetic storms. *J. Geophys. Res. Sp. Phys.* **2022**, *127*, e2021JA030169. [CrossRef]
5. Booker, H.G.; Wells, H.W. Scattering of radio waves by the F-region of the ionosphere. *J. Geophys. Res. Sp. Phys.* **1938**, *43*, 249–256. [CrossRef]
6. Kelley, M.C. *The Earth's Ionosphere: Plasma Physics & Electrodynamics*, 2nd ed.; International Geophysics Series; Academic Press: San Diego, CA, USA, 2009; ISBN 978-0-12-088425-4.
7. Abdu, M. Outstanding problems in the equatorial ionosphere–thermosphere electrodynamics relevant to spread F. *J. Atmos. Sol. Terr. Phys.* **2001**, *63*, 869–884. [CrossRef]
8. Huang, C.S.; Foster, J.C.; Sahai, Y. Significant depletions of the ionospheric plasma density at middle latitudes: A possible signature of equatorial spread *F* bubbles near the plasmapause. *J. Geophys. Res. Sp. Phys.* **2007**, *112*, D12. [CrossRef]
9. Dymond, K.F. Global observations of L band scintillation at solar minimum made by COSMIC. *Radio Sci.* **2012**, *47*, 1–10. [CrossRef]
10. Aa, E.; Zou, S.; Liu, S. Statistical analysis of equatorial plasma irregularities retrieved from swarm 2013–2019 observations. *J. Geophys. Res. Sp. Phys.* **2020**, *125*, e2019JA027022. [CrossRef]
11. Afolayan, A.O.; Singh, M.J.; Abdullah, M.; Buhari, S.M.; Yokoyama, T.; Supnithi, P. Observation of seasonal asymmetry in the range spread F occurrence at different longitudes during low and moderate solar activity. *Ann. Geophys.* **2019**, *37*, 733–745. [CrossRef]
12. Ye, H.; Xue, X.; Yu, T.; Sun, Y.Y.; Yi, W.; Long, C.; Zhang, W.; Dou, X. Ionospheric F-layer scintillation variabilities over the american sector during sudden stratospheric warming events. *Sp. Weather* **2021**, *19*, e2020SW002703. [CrossRef]
13. Yeh, K.C.; Liu, C.H. Radio wave scintillations in the ionosphere. *Proc. IEEE* **1982**, *70*, 324–360. [CrossRef]
14. Zakharenkova, I.; Cherniak, I. Underutilized spaceborne GPS observations for space weather monitoring. *Sp. Weather* **2018**, *16*, 345–362. [CrossRef]

15. Kuai, J.; Wang, K.; Zhong, J.; Wan, X.; Huang, F.; Sun, H.; Chen, J.; Song, X.; Han, H. Analysis of the ionospheric irregularities and phase scintillation at low and middle latitudes based on swarm observations. *Remote Sens.* **2022**, *14*, 4780. [CrossRef]
16. Chang, H.; Kil, H.; Sun, A.K.; Zhang, S.R.; Lee, J. Ionospheric disturbances in low- and midlatitudes during the geomagnetic storm on 26 August 2018. *J. Geophys. Res. Sp. Phys.* **2022**, *127*, e2021JA029879. [CrossRef]
17. Ma, G.; Maruyama, T. A super bubble detected by dense GPS network at east Asian longitudes. *Geophys. Res. Lett.* **2006**, *33*, 1–5. [CrossRef]
18. Cherniak, I.; Zakharenkova, I. First observations of super plasma bubbles in Europe. *Geophys. Res. Lett.* **2016**, *43*, 11137–11145. [CrossRef]
19. Katamzi-Joseph, Z.T.; Habarulema, J.B.; Hernández-Pajares, M. Midlatitude postsunset plasma bubbles observed over Europe during intense storms in April 2000 and 2001. *Sp. Weather* **2017**, *15*, 1177–1190. [CrossRef]
20. Aa, E.; Huang, W.; Liu, S.; Ridley, A.; Zou, S.; Shi, L.; Chen, Y.; Shen, H.; Yuan, T.; Li, J.; et al. Midlatitude plasma bubbles over china and adjacent areas during a magnetic storm on 8 September 2017. *Sp. Weather* **2018**, *16*, 321–331. [CrossRef]
21. Martinis, C.; Baumgardner, J.; Mendillo, M.; Wroten, J.; Coster, A.; Paxton, L. The night when the auroral and equatorial ionospheres converged. *J. Geophys. Res. Sp. Phys.* **2006**, *111*, 8085–8095. [CrossRef]
22. Sori, T.; Shinbori, A.; Otsuka, Y.; Tsugawa, T.; Nishioka, M.; Yoshikawa, A. Generation mechanisms of plasma density irregularity in the equatorial ionosphere during a geomagnetic storm on 21–22 December 2014. *J. Geophys. Res. Sp. Phys.* **2022**, *127*, e2021JA030240. [CrossRef]
23. Yizengaw, E.; Groves, K.M. Longitudinal and seasonal variability of equatorial ionospheric irregularities and electrodynamics. *Sp. Weather* **2018**, *16*, 946–968. [CrossRef]
24. Li, G.; Ning, B.; Wang, C.; Abdu, M.A.; Otsuka, Y.; Yamamoto, M.; Wu, J.; Chen, J. Storm-enhanced development of postsunset equatorial plasma bubbles around the meridian 120° E/60° W on 7–8 September 2017. *J. Geophys. Res. Sp. Phys.* **2018**, *123*, 7985–7998. [CrossRef]
25. Rajesh, P.K.; Lin, C.C.H.; Lin, J.T.; Lin, C.Y.; Liu, J.Y.; Matsuo, T.; Huang, C.Y.; Chou, M.Y.; Yue, J.; Nishioka, M.; et al. Extreme Poleward expanding super plasma bubbles over Asia-Pacific region triggered by Tonga Volcano eruption during the recovery-phase of geomagnetic storm. *Geophys. Res. Lett.* **2022**, *49*, e2022GL099798. [CrossRef]
26. Sun, L.; Xu, I.; Wang, W.; Yue, X.; Yuan, W.; Ning, B.; Zhang, D.; de Meneses, F.C. Mesoscale field-aligned irregularity structures (FAIs) of airglow associated with medium-scale traveling ionospheric disturbances (MSTIDs). *J. Geophys. Res. Sp. Phys.* **2015**, *120*, 9839–9858. [CrossRef]
27. Huang, F.; Lei, J.; Dou, X.; Luan, X.; Zhong, J. Nighttime medium-scale traveling ionospheric disturbances from airglow imager and global navigation satellite systems observations. *Geophys. Res. Lett.* **2018**, *45*, 31–38. [CrossRef]
28. Sivakandan, M.; Mondal, S.; Sarkhel, S.; Chakrabarty, D.; Sunil Krishna, M.V.; Upadhayaya, A.K.; Shinbori, A.; Sori, T.; Kannaujiya, S.; Champati Ray, P.K. Evidence for the in-situ generation of plasma depletion structures over the transition region of geomagnetic low-mid latitude. *J. Geophys. Res. Sp. Phys.* **2021**, *126*, e2020JA028837. [CrossRef]
29. Wei, L.; Jiang, C.; Lan, T.; Wang, W.; Shen, H.; Aa, E.; Huang, W.; Liu, J.; Yang, G.; Hu, Y.; et al. Observations of unusual daytime range spread F at middle latitude during the afternoon hours. *Sp. Weather* **2021**, *19*, e2021SW002870. [CrossRef]
30. Li, G.; Ning, B.; Zhao, B.; Liu, L.; Wan, W.; Ding, F.; Xu, J.S.; Liu, J.Y.; Yumoto, K. Characterizing the 10 November 2004 storm-time middle-latitude plasma bubble event in Southeast Asia using multi-instrument observations. *J. Geophys. Res. Sp. Phys.* **2009**, *114*, 1–16. [CrossRef]
31. Nishioka, M.; Saito, A.; Tsugawa, T. Super-medium-scale traveling ionospheric disturbance observed at midlatitude during the geomagnetic storm on 10 November 2004. *J. Geophys. Res. Sp. Phys.* **2009**, *114*, 1–16. [CrossRef]
32. Park, J.; Stolle, C.; Xiong, C.; Lühr, H.; Pfaff, R.F.; Buchert, S.; Martinis, C.R. A dayside plasma depletion observed at midlatitudes during quiet geomagnetic conditions. *Geophys. Res. Lett.* **2015**, *42*, 967–974. [CrossRef]
33. Park, J.; Kil, H.; Stolle, C.; Lühr, H.; Coley, W.R.; Coster, A.; Kwak, Y.S. Daytime midlatitude plasma depletions observed by Swarm: Topside signatures of the rocket exhaust. *Geophys. Res. Lett.* **2016**, *43*, 1802–1809. [CrossRef]
34. Yang, Z.; Morton, Y.T.J.; Zakharenkova, I.; Cherniak, I.; Song, S.; Li, W. Global view of ionospheric disturbance impacts on kinematic GPS positioning solutions during the 2015 St. Patrick's Day Storm. *J. Geophys. Res. Sp. Phys.* **2019**, *125*, e2019JA027681. [CrossRef]
35. Xiong, B.; Wan, W.; Yu, Y.; Hu, L. Investigation of ionospheric TEC over China based on GNSS data. *Adv. Sp. Res.* **2016**, *58*, 867–877. [CrossRef]
36. Sori, T.; Shinbori, A.; Otsuka, Y.; Tsugawa, T.; Nishioka, M. Characteristics of GNSS total electron content enhancements over the midlatitudes during a geomagnetic storm on 7 and 8 November 2004. *J. Geophys. Res. Sp. Phys.* **2019**, *124*, 10376–10394. [CrossRef]
37. Sori, T.; Shinbori, A.; Otsuka, Y.; Tsugawa, T.; Nishioka, M. The occurrence feature of plasma bubbles in the equatorial to midlatitude ionosphere during geomagnetic storms using long-term GNSS-TEC data. *J. Geophys. Res. Sp. Phys.* **2021**, *126*, e2020JA029010. [CrossRef]
38. Dao, T.; Otsuka, Y.; Shiokawa, K.; Nishioka, M.; Yamamoto, M.; Buhari, S.M.; Abdullah, M.; Husin, A. Coordinated observations of postmidnight irregularities and thermospheric neutral winds and temperatures at low latitudes. *J. Geophys. Res. Sp. Phys.* **2017**, *122*, 7504–7518. [CrossRef]

39. Buhari, S.M.; Abdullah, M.; Hasbi, A.M.; Otsuka, Y.; Yokoyama, T.; Nishioka, M.; Tsugawa, T. Continuous generation and two-dimensional structure of equatorial plasma bubbles observed by high-density GPS receivers in Southeast Asia. *J. Geophys. Res. Sp. Phys.* **2014**, *119*, 10569–10580. [CrossRef]
40. Yeh, H.C.; Su, S.Y.; Yeh, Y.C.; Wu, J.M.; Heelis, R.A.; Holt, B.J. Scientific mission of the IPEI payload onboard ROCSAT-1. *Terr. Atmos. Ocean. Sci.* **1999**, *10*, 19–42. [CrossRef]
41. Xiong, C.; Park, J.; Lühr, H.; Stolle, C.; Ma, S.Y. Comparing plasma bubble occurrence rates at CHAMP and GRACE altitudes during high and low solar activity. *Ann. Geophys.* **2010**, *28*, 1647–1658. [CrossRef]
42. Keskinen, M.J.; Ossakow, S.L. Theories of high-latitude ionospheric irregularities: A review. *Radio Sci.* **1983**, *18*, 1077–1091. [CrossRef]
43. Tsunoda, R.T. High-latitude F region irregularities: A review and synthesis. *Rev. Geophys.* **1988**, *26*, 719–760. [CrossRef]
44. Zhao, B.; Wan, W.; Tschu, K.; Igarashi, K.; Kikuchi, T.; Nozaki, K.; Watari, S.; Li, G.; Paxton, L.J.; Liu, L.; et al. Ionosphere disturbances observed throughout Southeast Asia of the superstorm of 20-22 November 2003. *J. Geophys. Res. Sp. Phys.* **2008**, *113*, 1–16. [CrossRef]
45. Shi, J.K.; Wang, G.J.; Reinisch, B.W.; Shang, S.P.; Wang, X.; Zherebotsov, G.; Potekhin, A. Relationship between strong range spread F and ionospheric scintillations observed in Hainan from 2003 to 2007. *J. Geophys. Res.* **2011**, *116*, A08306. [CrossRef]
46. Wang, Z.; Shi, J.K.; Torkar, K.; Wang, G.J.; Wang, X. Correlation between ionospheric strong range spread F and scintillations observed in Vanimo station. *J. Geophys. Res. Sp. Phys.* **2014**, *119*, 8578–8585. [CrossRef]
47. Jiang, C.; Yang, G.; Liu, J.; Yokoyama, T.; Komolmis, T.; Song, H.; Lan, T.; Zhou, C.; Zhang, Y.; Zhao, Z. Ionosonde observations of daytime spread F at low latitudes. *J. Geophys. Res. Sp. Phys.* **2016**, *121*, 12093–12103. [CrossRef]
48. Wei, L.; Jiang, C.; Hu, Y.; Aa, E.; Huang, W.; Liu, J.; Yang, G.; Zhao, Z. Ionosonde observations of spread F and spread Es at low and middle latitudes during the recovery phase of the 7–9 September 2017 geomagnetic storm. *Remote Sens.* **2021**, *13*, 1010. [CrossRef]
49. Tsunoda, R.T. Satellite traces: An ionogram signature for large-scale wave structure and a precursor for equatorial spread F. *Geophys. Res. Lett.* **2008**, *35*, 2–5. [CrossRef]
50. Li, G.; Ning, B.; Abdu, M.A.; Yue, X.; Liu, L.; Wan, W.; Hu, L. On the occurrence of postmidnight equatorial F region irregularities during the June solstice. *J. Geophys. Res. Sp. Phys.* **2011**, *116*, A4. [CrossRef]
51. Huang, C.S.; De La Beaujardiere, O.; Roddy, P.A.; Hunton, D.E.; Ballenthin, J.O.; Hairston, M.R. Long-lasting daytime equatorial plasma bubbles observed by the C/NOFS satellite. *J. Geophys. Res. Sp. Phys.* **2013**, *118*, 2398–2408. [CrossRef]
52. Huang, C.S.; Le, G.; de La Beaujardiere, O.; Roddy, P.A.; Hunton, D.E.; Pfaff, R.F.; Hairston, M.R. Relationship between plasmabubbles and density enhancements: Observations and interpretation. *J. Geophys. Res. Sp. Phys.* **2014**, *119*, 1325–1336. [CrossRef]
53. Zhong, J.; Lei, J.; Yue, X.; Luan, X.; Dou, X. Middle-latitudinal band structure observed in the nighttime ionosphere. *J. Geophys. Res. Sp. Phys.* **2019**, *124*, 5857–5873. [CrossRef]
54. Cherniak, I.; Zakharenkova, I.; Sokolovsky, S. Multi-instrumental observation of storm-induced ionospheric plasma bubbles at equatorial and middle latitudes. *J. Geophys. Res. Sp. Phys.* **2019**, *124*, 1491–1508. [CrossRef]
55. Fejer, B.G.; Tracy, B.D.; Pfaff, R.F. Equatorial zonal plasma drifts measured by the C/NOFS satellite during the 2008–2011 solar minimum. *J. Geophys. Res. Sp. Phys.* **2013**, *118*, 3891–3897. [CrossRef]
56. Lühr, H.; Park, J.; Ritter, P.; Liu, H. In-situ CHAMP observation of ionosphere-thermosphere coupling. *Space Sci. Rev.* **2012**, *168*, 237–260. [CrossRef]
57. Sivakandan, M.; Martinis, C.; Otsuka, Y.; Chau, J.L.; Norrell, J.; Mielich, J.; Conte, J.F.; Stolle, C.; Rodríguez-Zuluaga, J.; Shinbori, A.; et al. On the role of E-F region coupling in the generation of nighttime MSTIDs during summer and equinox: Case studies over Northern Germany. *J. Geophys. Res. Sp. Phys.* **2022**, *127*, e2021JA030159. [CrossRef]
58. Yokoyama, T.; Hysell, D.L.; Otsuka, Y.; Yamamoto, M. Three-dimensional simulation of the coupled Perkins and E_s-layer instabilities in the nighttime midlatitude ionosphere. *J. Geophys. Res. Sp. Phys.* **2009**, *114*, A11. [CrossRef]
59. Yu, B.; Xue, X.; Yue, X.; Yang, C.; Yu, C.; Dou, X.; Ning, B.; Hu, L. The global climatology of the intensity of the ionospheric sporadic e layer. *Atmos. Chem. Phys.* **2019**, *19*, 4139–4151. [CrossRef]
60. Yu, B.; Scott, C.J.; Xue, X.; Yue, X.; Dou, X. Using GNSS radio occultation data to derive critical frequencies of the ionospheric sporadic E layer in real time. *GPS Solut.* **2021**, *25*, 1–12. [CrossRef]